Acta Crystallographica Section B
**Structural Science**
ISSN 0108-7681

# X-ray study and structure simulation of amorphous tungsten oxide

**L. A. Lugovskaya,[a]* L. A. Aleshina,[a] G. M. Kalibaeva[b] and A. D. Fofanov[a]**

[a]Petrozavodsk State University, pr. Lenina 33, 185014 Pertozavodsk, Russia, and [b]INFM e Dipartimento di Fisica della Universita degli Studi di Modena, Modena, Italy

Correspondence e-mail: liubovl@psu.karelia.ru

Received 4 December 2001
Accepted 16 April 2002

In this work, X-ray studies of the amorphous oxide films obtained by thermal evaporation of $WO_3$ powder in a vacuum and by anodic oxidation were carried out. X-ray diffraction patterns were obtained in the symmetric reflection geometry on a DRON-4 diffractometer (Mo $K_\alpha$ radiation, LiF monochromator) in automatic mode. Molecular dynamics simulation of amorphous tungsten oxide atomic configurations has been carried out in the micro-canonical ensemble (NVE) for $N = 208$ atoms and $N = 624$ atoms, in a cubic cell, using pairwise Born–Mayer interaction potentials and periodic boundary conditions. One of the purposes of the present work is to analyze the influence of the parameters and the cutoff of the interaction potentials on the interatomic distances. The values obtained in the molecular dynamics simulation for the pair functions $D(r)$ are compared with the experimental data for amorphous oxides in order to choose the most convenient aforesaid values. The values of the average interatomic distances and the coordination numbers obtained by both methods are also compared. The result shows that the tungsten subsystem can be well reproduced using the potential cutoff radius of about 4 Å, but the oxygen subsystem can be well reproduced when the cutoff of the potential for the W—O pairs is equal to 2.8 Å. The configuration built during the molecular dynamics experiment consists of distorted octahedra. These octahedra form chains, as in the $WO_3$ phases of type $ReO_3$, and hexagonal rings, of the same type as in the $WO_3(1/3)H_2O$ phase, when we extract (1/3)O at every $WO_3$ unit. The pair function $D(r)$ and scattering intensity $I(s)$ distribution curves calculated for simulation configurations show a satisfactory agreement with experiment.

## 1. Introduction

The reversible colouration-bleaching process in tungsten trioxide under the action of an applied electric field (the electrochromic effect) was discovered in 1969 (Deb, 1969) and has been the subject of numerous studies in science and technology.

The studies of non-crystalline $WO_3$ films obtained by various methods show that their electrochromic properties are essentially dependent on the conditions and the methods of their synthesis (Aleshina *et al.*, 1982, 1998; Fillipchenko *et al.*, 1980; Gorbunov *et al.*, 1981; Shiojri & Migano, 1980; Olevskii *et al.*, 1984; Falaras *et al.*, 1984; Paola *et al.*, 1978). We can assume that this effect is associated with a different short-range order of atomic arrangement.

The atomic and electronic structure of amorphous $WO_3$ were studied with the first principles density functional calculation by De Wijs & De Groot (1999) for stoichiometric

amorphous $WO_3$ and the form with oxygen deficiency ($WO_{3-1/4}$). The authors have shown that the oxygen deficiency does not significantly affect the nearest-neighbour distances; nevertheless, it results in the appearance of very short W—W distances. The authors have considered small configuration $WO_3$ (8 W + 24 O and 27 W + 81 O) and have not compared the numeric results with experimental data. In Belaschenko (1994), amorphous and liquid $(Na_2O)_x(WO_3)_{1-x}$ were simulated by continuous static relaxation and molecular dynamics methods. The system with $x = 0$ corresponds to the $WO_3$ phase. It was found (Belaschenko, 1994) that all distances for models were considerably shorter than experimental data for amorphous $WO_3$ films.

In the present work, we report the results obtained by X-ray studies of the amorphous oxide films and by computer simulation of the stoichiometric $WO_3$ model and the model with oxygen excess ($WO_{3+1/3}$).

One of the purposes of the present work is to analyze the influence of the parameters and the cutoff of the interaction potentials on the interatomic distances. We compare the values obtained in the molecular dynamics simulation for the pair functions $D(r)$ with the experimental data for amorphous oxides in order to choose the most convenient aforesaid values. We also compare the values of the average interatomic distances and the coordination numbers obtained by both methods.

## 2. Experimental method

We have studied amorphous $WO_3$ films produced by two methods: by thermal evaporation of $WO_3$ powder in a vacuum with deposition on glass substrates and by anodization (Aleshina *et al.*, 1982). The anodic amorphous tungsten oxide was formed on poly- and single-crystal tungsten substrates in 0.01% $H_3PO_4$ at forming voltage $U_f = 120$ V and current density $j = 1$ mA cm$^{-2}$. The time of oxide formation was 40 min (Aleshina & Lugovskaya, 1997). Then, some films were separated from the metallic substrates and used for preparing powder specimens.

X-ray diffraction patterns were obtained in the symmetric reflection geometry on a DRON-4 diffractometer (Mo $K_\alpha$ radiation, LiF monochromator) in automatic mode. The maximum magnitude of the diffraction vector $s$ ($s = 4\pi \sin\theta/\lambda$) was 16.5 Å$^{-1}$ for powder specimens and 6.5 Å$^{-1}$ for oxide films on metallic and glass substrates.

Self-background, scattering air and scattering substrate corrections were subtracted from the measured intensities. Then absorption and polarization corrections were introduced and the experimental curves were normalized. The scattering intensities $I(s)$ (in electron units) were the same for the films on the substrates and for the powders.

Using the experimental curves $I(s)$, the $s$-weighting interference functions $H(s)$ were calculated, and they were used as the integrands for calculating the distribution curve of the pair functions $D(r)$ (Finbak & Borgen, 1954; Warren, 1969) in the form $H(s) = s\, i(s) \exp(-a^2 s^2)$, where $i(s)$ is the interference scattering function and $\exp(-a^2 s^2)$ is the attenuation factor. The methods for introducing various corrections to the experimental curves and for calculating $H(s)$ and $D(r)$ are considered elsewhere (Aleshina *et al.*, 1986; Aleshina & Fofanov, 1987).

The coordination numbers $N_{ij}$ from the distribution curves of the pair functions at given values of the radii $r_{ij}$ of the coordination spheres and their dispersions $\sigma_{ij}$ were determined by the method of singular expansion (Forsythe *et al.*, 1977; Lawson & Hanson, 1974). The $r_{ij}$ and $\sigma_{ij}$ values were obtained using the method of successive approximations, so the discrepancy between the experimental curve and the curve obtained from the set of $N_{ij}$, $r_{ij}$ and $\sigma_{ij}$ did not exceed 5% (Aleshina *et al.*, 1986; Aleshina & Fofanov, 1987). The types of experimental errors and their effect on the $D(r)$ curve were determined using the inverse Fourier transform (Aleshina *et al.*, 1995).

## 3. Experimental results

The distribution curves $H(s)$ and $D(r)$ calculated from the experimental data are shown in Figs. 1and 2.

Different experimental data for the deposited and anodic oxides (Figs. 1 and 2) show that anodic oxidation and thermal evaporation lead to the formation of amorphous tungsten oxides with different atomic structures.

Experimental data analysis was carried out taking into account the fact that the tungsten trioxide forms have a number of polymorphous modifications related to a more or less distorted $ReO_3$ structure type and consisting of corner-sharing $WO_6$ octahedra. These are cubic (Palatnic *et al.*, 1973), tetragonal, monoclinic and triclinic (Udalova & Klechkovskaya, 1986) modifications. In addition to these modifications, we have a hexagonal $WO_3$ phase, first synthesized by dehydration of $WO_3(1/3)H_2O$ (Gerand *et al.*, 1979). Later, hexagonal crystals of this phase were also obtained in the synthesis of anodic oxide films (Falaras *et al.*, 1984).

In all $ReO_3$ phases, the $WO_3$ octahedra form chains along three crystallographic coordinate axes (Figs. 3*a* and 3*b*). The

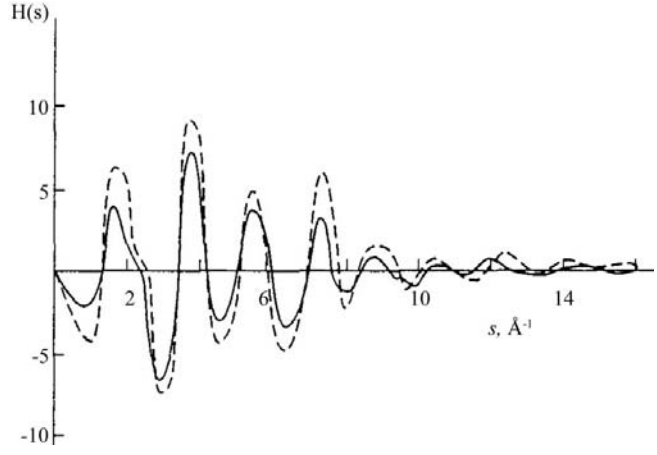


**Figure 1**
$H(s)$ functions for amorphous $WO_3$ oxides. The solid line indicates the experimental data for the anodic oxide, and the dashed line indicates the data for the deposited film.

phase transitions between these modifications can be classified as 'deformation transitions', because they proceed without bond breaking and are accompanied by the distortion of the octahedra, the displacement of W atoms from their centres and the inclination of these octahedra with respect to the axes corresponding to an ideal cubic structure of the $ReO_3$ type. The deformation of the octahedra results in a lowering of the symmetry and a twofold, fourfold or eightfold increase in the unit-cell's dimension with respect to the cubic cell (Udalova & Klechkovskaya, 1986). The W—O chains acquire a zigzag shape (Fig. 3*b*). Interatomic distance variation analysis of the different $ReO_3$-type phases (Aleshina *et al.*, 1982; Aleshina & Lugovskaya, 1997; Lugovskaya, 2000) indicates that discrepancies occur even for the shortest W—O distances.

The coordination polyhedron of the hexagonal $WO_3$ modification is also an octahedron (Gerand *et al.*, 1979), and the $WO_6$ octahedra not only share their vertices but also form a structural pattern different from that characteristic of the $ReO_3$ phases (Fig. 3*c*). In the hexagonal modification, the octahedra form six-membered rings in the layers perpendicular to [00l].

The distribution of atoms over the coordination spheres in this phase differs from the characteristic distribution for the $ReO_3$ phases: first, the coordination numbers are different, and second, there are no W—W pairs between the W—O spheres (Aleshina & Lugovskaya, 1997; Lugovskaya, 2000).

The hexagonal $WO_3$ phase and the $WO_3(1/3)H_2O$ phase are pseudomorphic and are related by the following orientational relationships (Gerand *et al.*, 1981):

[100] $WO_3(1/3)H_2O$ || [100] hex $WO_3$

[001] $WO_3(1/3)H_2O$ || [001] hex $WO_3$.

In Fig. 4, we can see the structure of the $WO_3(1/3)H_2O$ phase and the interatomic distances.

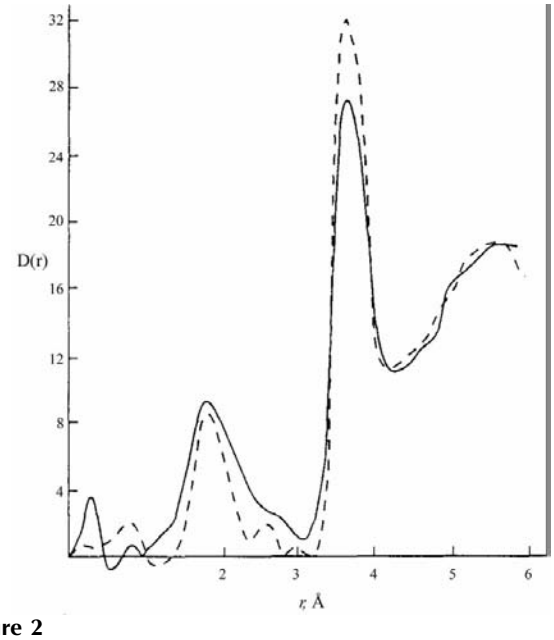


**Figure 2**
The distribution curve of pair functions $D(r)$ for amorphous $WO_3$ oxides. The solid line indicates the experimental data for the anodic oxide, and the dashed line indicates the data for the deposited film.

The results of the numerical calculation of the atomic distribution through coordination spheres for all the mentioned phases are briefly described by Aleshina & Lugovskaya (1997) and Lugovskaya (2000). The comparison of these results with the values of the coordination numbers $N_{ij}$ and coordination sphere radii determined from the experimental distribution curves of pair functions $D(r)$ for the anodic oxide showed that the arrangement of W and O atoms corresponds to the characteristic configuration of the crystalline $WO_3(1/3)H_2O$ modification. Table 1 shows the calculated characteristics of the short-range order for the amorphous

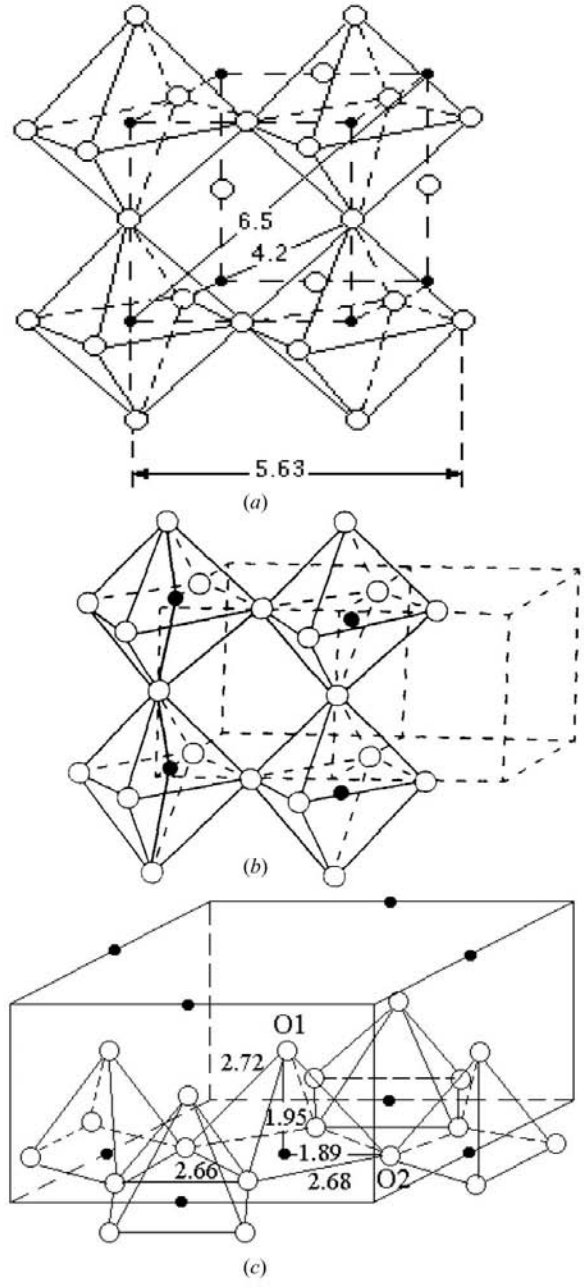


**Figure 3**
The structural motif of the arrangement of octahedra in the (*a*) cubic, (*b*) orthorhombic and (*c*) hexagonal phases of tungsten trioxide.

**Table 1**
Short-range-order characteristics calculated from experimental pair functions $D(r)$ for the amorphous anodic oxide films, and the data for the corresponding crystalline phase $WO_3(1/3)H_2O$.

Note: 3.0% discrepancy. $\Delta r_{ij} = \pm 0.01$ Å, $\Delta\sigma_{ij} = \pm 0.02$ Å.

| | | | | | Crystal | | |
|---|---|---|---|---|---|---|---|
| | | Amorphous specimen (experiment) | | | Without the hydrogen bonds | | Taking into account the hydrogen bonds |
| Coordination sphere | Sphere type | $r_{ij}$ (Å) | $N_{ij} \pm \Delta N_{ij}$ (atoms) | $\sigma_{ij}$ (Å) | $\langle r_{ij} \rangle$ (Å) | $N_{ij}^{cr}$ (atoms) | $N_{ij}^{cr}$ (atoms) |
| 1 | W—O | 1.85 | 5.4 ± 0.01 | 0.23 | 1.91 ± 0.06 | 5.7 | 5.7 |
| 2 | W—O | 2.22 | 1.6 ± 0.05 | 0.14 | 2.08 ± 0.01 | 0.3 | 0.3 |
| 3 | O—O | 2.65 | 17.0 ± 0.6 | 0.30 | 2.74 ± 0.41 | 8.4 | 11.3 |
| 4 | W—W | 3.72 | 4.0 ± 0.3 | 0.25 | 3.66 ± 0.11 | 4.3 | 4.3 |
| 5 | W—W | 3.81 | 1.4 ± 0.3 | 0.21 | 3.85 ± 0.04 | 1.3 | 1.4 |
| 6 | W—O | 4.20 | 12.0 ± 1.7 | 0.40 | 4.09 ± 0.18 | 13.2 | 13.2 |
| 7 | W—O | 4.42 | 10.0 ± 1.9 | 0.31 | 4.46 ± 0.25 | 10.9 | 11.4 |
| 8 | W—W | 5.08 | 7.5 ± 0.3 | 0.49 | 5.12 ± 0.26 | 7.5 | 7.5 |
| 9 | W—W | 5.60 | 3.8 ± 0.2 | 0.30 | 5.62 ± 0.16 | 3.3 | 3.3 |
| 10 | W—O | 5.98 | 24.0 ± 1.0 | 0.27 | 5.99 ± 0.23 | 12.9 | 13.3 |
| 11 | W—W | 6.32 | 4.5 ± 0.4 | 0.42 | 6.32 ± 0.11 | 4.4 | 4.4 |
| 12 | W—O | 6.58 | 28.0 ± 1.5 | 0.30 | 6.60 ± 0.25 | 24.6 | 26.0 |

anodic oxide obtained from the experimental $D(r)$ pair functions normalized to the $WO_3(1/3)H_2O$ composition and for the corresponding crystalline phase.

The maximum discrepancy is observed for the third (O—O) and the tenth (W—O) spheres. In the $WO_3(1/3)H_2O$ crystalline structure, there are two types of octahedra (Gerand *et al.*, 1981): a regular octahedron with the W—O bond equal to 1.93 Å and a distorted octahedron with one shortened W—O bond (1.84 Å) and one elongated W—$H_2O$ bond (2.08 Å). Since the number of elongated bonds (the second W—O sphere) for the considered amorphous sample is somewhat overestimated compared with that for the crystal, the corresponding coordination numbers for the crystalline phase taking into account the hydrogen bonding (Table 1) were calculated. The contributions of the W—H, O—H and H—H atomic pairs to the coordination numbers of the W—O, W—W and O—O spheres, disregarding the H atoms, were calculated by the method suggested by Aleshina & Nikitina (1992). The coordinates of the H atoms were calculated proceeding from the positions of water molecules in the $WO_3(1/3)H_2O$ lattice [Gerand *et al.* (1981) indicate the position of the O atom in this molecule]. The O—H bond length was taken to be 0.97 Å, and the H—O—H angle was taken to be 105°, following the data given by Bokii (1971) for $H_2O$. For this configuration of H atoms, the main changes in the coordination numbers are associated with the O—O sphere, so the $N_{O-O}$ value increases from 8.4 atoms to 11.7 atoms. The coordination numbers for the W—O spheres change considerably only at the seventh, tenth and twelfth spheres. Taking into account the contribution of the W—H, O—H and H—H pairs of atoms to the coordination numbers makes the $N_{ij}$ calculated for the $WO_3(1/3)H_2O$ oxide and those obtained experimentally more consistent.

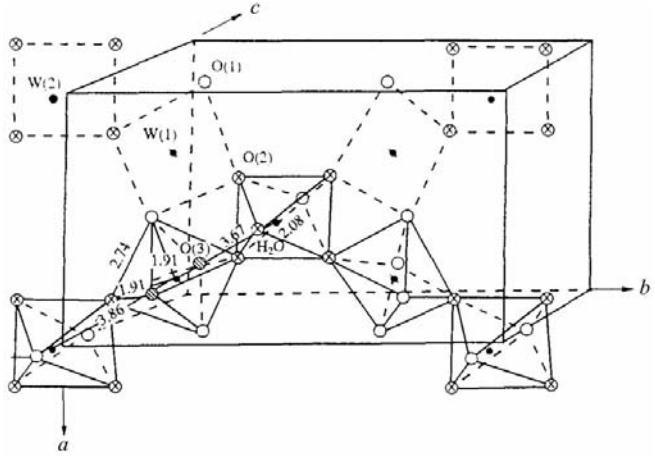


**Figure 4**
The structural motif of the arrangement of octahedra in the orthorhombic phase $WO_3(1/3)H_2O$.

Thus, the X-ray study of the amorphous anodic tungsten oxide formed in the $H_3PO_4$-based electrolyte showed that the arrangement of W and O atoms corresponds to the configuration characteristic of the crystalline $WO_3(1/3)H_2O$ phase.

Overestimated coordination numbers at the first and second coordination spheres can probably be interpreted in terms of additional substitution of O atoms by OH groups or $H_2O$ molecules in the lattice, with the basic $WO_3(1/3)H_2O$-type of the structure being preserved (Aleshina & Lugovskaya, 1997; Lugovskaya, 2000).

For the oxide films obtained by thermal evaporation of $WO_3$ powder in a vacuum, the values of the coordination number $N_{ij}$ and coordination sphere radii determined from the experimental distribution curves of pair functions $D(r)$ are close to those calculated for the orthorhombic phase of $WO_3$ (Table 2) (Aleshina *et al.*, 1982).

The coordination sphere for the $WO_3$ oxide obtained by thermal evaporation of $WO_3$ powder in a vacuum spreads much less than that for the anodic $WO_3$ oxide (Tables 1 and 2). The value of the dispersion $\sigma_{ij}$ for the first coordination sphere

**Table 2**
Short-range-order characteristics calculated from experimental $D(r)$ pair functions for the amorphous oxide films obtained by thermal evaporation of $WO_3$ powder in a vacuum, and the data for the corresponding crystalline $ReO_3$-type phases.

Note: 3.0% discrepancy. $\Delta r_{ij} = \pm 0.01$ Å, $\Delta\sigma_{ij} = \pm 0.02$ Å.

| | | Amorphous† | | | Crystalline orthorhombic | | | Crystalline monoclinic | | |
|---|---|---|---|---|---|---|---|---|---|---|
| Coordination sphere | Type of sphere | $r_{ij}$ (Å) | $N_{ij} \pm \Delta N_{ij}$ (atoms) | $\sigma_{ij}$ (Å) | $\langle r_{ij}\rangle$ (Å) | $N^s_{ij}$ (atoms) | $\Delta r_{ij}$ (Å) | $\langle r_{ij}\rangle$ (Å) | $N^s_{ij}$ (atoms) | $\Delta r_{ij}$ (Å) |
| 1 | W—O | 1.88 | $5.0 \pm 0.2$ | 0.12 | 1.88 | 6.0 | 0.03 | 1.90 | 6.0 | 0.19 |
| 3 | O—O | 2.65 | $8.5 \pm 2.0$ | 0.10 | 2.64 | 8.0 | 0.20 | 2.64 | 8.0 | 0.16 |
| 4 | W—W | 3.72 | $5.8 \pm 0.5$ | 0.28 | 3.76 | 6.0 | 0.06 | 3.78 | 6.0 | 0.06 |
| 6 | W—O | 3.94 | $13.0 \pm 2.0$ | 0.35 | 3.93 | 14.0 | 0.11 | – | – | – |
| 7 | W—O | 4.58 | $12.0 \pm 2.0$ | 0.15 | 4.42 | 8.0 | 0.05 | 4.21 | 24.0 | 0.39 |
| 8 | W—W | 5.04 | $5.0 \pm 0.5$ | 0.40 | 4.96 | 6.0 | 0.05 | 4.98 | 6.0 | 0.07 |

† Aleshina & Lugovskaya (1997).

is close to the sum of the widths due to thermal vibrations and scattering ($\Delta r_1$) in the crystal for the orthorhombic phase (Table 2).

Such a small dispersion allows us to suppose that the $WO_3$ oxide films obtained by thermal evaporation of $WO_3$ powder in a vacuum are quasi-amorphous, *i.e.* they are polycrystalline with a very small grain size.

For this model, the scattering intensity can be calculated using the Debye formula for the case when the crystallites have the shape of parallelepipeds (Aleshina *et al.*, 1982). The calculations were carried out for all the polymorph modifications of the $WO_3$ oxides. Using various combinations of the parallelepiped edge lengths, we minimized the difference $|H(s)_{\rm calc} - H(s)_{\rm exp}|$.

The best agreement with experiment was obtained for the $WO_3$ orthorhombic phase, having the shape of a parallelepiped with dimensions $2a \times b \times 5c$ ($\simeq 15 \times 8 \times 20$ Å). Suitable $H(s)$ curves are presented in Fig. 5.

Thus, $WO_3$ films obtained by thermal evaporation in a vacuum have a quasi-amorphous structure. The structure is characterized by the presence of crystallites shaped mainly as orthorhombic-phase parallelepipeds with dimensions $15 \times 8 \times 20$ Å.

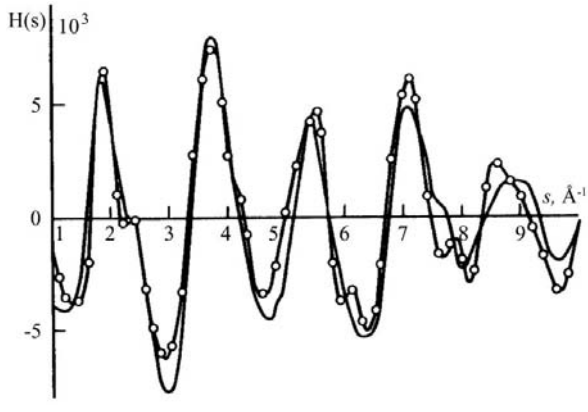


**Figure 5**
The function $H(s)$ for $WO_3$. The lines with points correspond to the experimental data for the $WO_3$ oxide films obtained by thermal evaporation of $WO_3$ powder in a vacuum. The lines without points are calculated from the Debye formula for the case when the crystallites have the shape of a parallelepiped for the orthorhombic modification of $WO_3$.

It is not possible to obtain the atomic coordinates in the short-range-order area from X-ray analysis; therefore, in the present work, the computer simulation of the tungsten oxide structure was carried out by the molecular dynamics method.

## 4. Molecular dynamics simulation

The molecular dynamics simulation was carried out in the micro-canonical ensemble (NVE) (Andersen, 1980), which keeps constant the number of particles, the volume and the total energy of the system. This ensemble is considered reasonable at simulating phase transitions in crystals and amorphous alloys (Parinello & Rahman, 1981; Stepanyuk, Katsnelson *et al.*, 1991; Stepanyuk, Szasz *et al.*, 1991) and oxides (Belaschenko, 1994; Buhtoiarov & Voronova, 1989; Gutierrez & Johansson, 2002; Gutierrez *et al.*, 2000) and does not require long calculation times. Thus, it has been used frequently in the past. The leap-frog method was used to integrate the classical equations of motion (Hockney & Eastwood, 1981; Kalibaeva, 1992).

The stability condition for this scheme is $\omega dt < 2$ (Hockney & Eastwood, 1981), where $\omega$ is the maximum frequency of the system oscillations. Usually, it can be estimated by the Debye frequency, $\omega D = 2\pi k_{\rm B}\theta/h$, where $k_{\rm B}$ is the Boltzmann constant, $\theta$ is the characteristic Debye temperature and $h$ is Planck's constant.

The order of the Debye frequency can be estimated from the Debye temperature by the formula

$$\theta = \frac{3h}{2\pi r_s x_m}\left(\frac{T_m}{Mk_{\rm B}}\right)^{1/2},$$

where $x_m$ is the atomic displacement (about 0.2–0.25 Å for solids), $r_s$ is the average radius of the unit cell, $T_m$ is the melting temperature and $M$ is the molar mass. Estimated this way, the Debye frequency for tungsten oxide is about $10^{13}$ s$^{-1}$ (Lugovskaya, 2000).

The time step for the integration of the equations of motion was taken to be $t = 10^{-15}$ s, which guarantees the stability of that scheme.

The Born–Mayer interaction potential was used to simulate the structure of the tungsten trioxide:

$$V = q_i q_j r^{-1} + A_{ij} \exp(-r\rho_{ij}^{-1}).$$

For the W—O, O—O and W—W interaction potential calculations, two sets of coefficients were used.

The values of the coefficients calculated for the new molecular mechanics force field, the Universal force field (UFF), suggested by Rappe *et al.* (1992) and taken from Belaschenko (1994), are shown in Table 3.

In Belaschenko (1994), the $A_{ij}$ were chosen to be equal to 1.8 Å for the interatomic distance W—O. The W—W interaction was considered as a purely Coulomb interaction.

It was determined (Lugovskaya, 2000) that the values of the potentials calculated with this set of coefficients were reasonable. A small discrepancy within the range from $\rho_{ij}$ to 1 Å does not affect the results of the atomic configuration calculations: with just the same values of effective charges and potential cutoff, we have not observed any considerable differences between the $D(r)$ curves.

To reduce the boundary effects, periodic boundary conditions were used. It was considered that each atom was interacting only with the atoms inside the cutoff. If the atom is near the border of the calculation cell, it also interacts with the atoms of the next projection of the cell (Kalibaeva, 1992).

All the molecular dynamics calculations were carried out for the two-component W—O system at the respective component concentration.

The coordinates of the O and W atoms in the initial configurations correspond to the atomic arrangement in the crystalline $WO_3$ cubic phase and $WO_3(1/3)H_2O$ (without H atoms).

First, melting was simulated by raising the cluster temperature higher than the melting temperature of the oxide (3000 K) (for different phases of tungsten oxide the melting temperature varies between 1746 K and 2300 K) at $10^{15}$ K s$^{-1}$. The melted cluster was stabilized over 10 000 time steps at 2300 K, then it was cooled down to room temperature (300 K) over 2000 time steps. The output was recorded each 20 time steps. Further, the system was relaxed at room temperature over 30 000 time steps to reach an equilibrium state.

Using the atomic coordinates of the configuration obtained at the different phases of the simulation by the modified Debye formula, we can obtain (Skrishevskii, 1980; Fofanov, 1998)

$$I(s) = \frac{1}{N_f}\left[\sum_{i=1}^{N} f_i^2 + 2\sum_{i}^{N-1}\sum_{j=i+1}^{N}\frac{1}{2}\left(f_i f_j^* + f_i^* f_j\right)\frac{\sin(sr_{ij})}{sr_{ij}}\exp(-0.5\sigma_{ij}^2 s^2)\right],$$

where $f_i$ and $f_j$ are the atomic scattering functions, $N$ is the number of particles for the considered configuration, $\sigma_{ij}$ is the dispersion of interatomic distances about the average value $r_{ij}$, and $N_f$ is the number of the formula units at the atomic configuration.

The model configuration scattering intensities calculated in this way were used to calculate $s$-weighting interference functions $H(s)$ and the distribution curves of the pair functions $D(r)$. These functions were compared with the experimental data for $D(r)$.

**Table 3**
Coefficients for the potentials.

| | $A_{ij}$ (eV)† | $\rho_{ij}$ (Å)† | $A_{ij}$ (eV)‡ | $\rho_{ij}$ (Å)‡ |
|---|---|---|---|---|
| W—W | 473.182 | 0.256 | – | 0.29 |
| O—O | 2529.764 | 0.249 | 1500 | 0.29 |
| W—O | 4382.444 | 0.258 | 3400 | 0.29 |

† Rappe *et al.* (1992). ‡ Belaschenko (1994).

In addition, the coordination numbers and the mean radii of the coordination spheres were calculated from the atomic coordinates of the configurations.

## 5. Results of the molecular dynamics simulation

Two types of initial configurations were formed on the basis of the crystal lattices: the cubic $WO_3$ phase ($a$ = 3.84 Å) and the orthorhombic $WO_3(1/3)H_2O$ phase without H atoms (space group $Fmm2$, $a$ = 7.359 Å, $b$ = 12.513 Å, $c$ = 7.704 Å). The initial orthorhombic configuration of the $WO_{3+1/3}$ phase was reduced to cubic form artificially so that the number of atoms and the density of the configuration were constant. Therefore, the order characteristic of the crystal was violated, and an element of chaos was introduced.

The densities of the models were varied from 6.0 g cm$^{-3}$ to 7.3 g cm$^{-3}$. The lower value corresponds to the density of the studied $WO_3$ films obtained by thermal evaporation of $WO_3$ powder in a vacuum; the density 7.3 g cm$^{-3}$ is that of the $WO_3$ monocrystals. The density of the amorphous anodic oxide $WO_3$ films was taken to be 6.5 g cm$^{-3}$.

### 5.1. $WO_3$ configuration

The $WO_3$ configuration consisted of 256 atoms (192 O atoms and 64 W atoms, 64 formula units of $WO_3$) placed inside a cube with linear dimensions dependent on model density.

At the initial stage of the simulation (melting), we obtained an atomic distribution disordered as much as possible. The distribution curves of the pair functions $D(r)$ for the melted (not-relaxed) initial configuration simulated for $WO_3$ (256 atoms) is presented in Fig. 6. Analysis of the effect on the values of effective charges was made.

At the first stage of the simulation (melting) and during the relaxation of the melted cluster, the W—O, W—W and O—O potentials calculated with effective charges $z_W = 3.36$ and $z_O = -1.12$ (Urusov, 1975) were used (ionic interaction degree 0.56). The cutoff of the interatomic potentials was one-quarter of the linear dimension of the model configuration.

It was detected that with these conditions the shape of the first maximum of the distribution curve $D(r)$ calculated for the melted relaxed configuration has exactly the same form as the experimental $D(r)$ curve (Fig. 7). However, the first maximum of the $D(r)$ curve obtained for the model configuration is displaced towards larger $r$ for $\Delta r_{W-O} = 0.4$ Å compared with the experimental curve. The maximum that corresponds to the W—W pairs is displaced towards lower $r$, but this time for

$\Delta r_{W-W} = 0.1$ Å. Using these conditions of relaxation, the interatomic O—O distances undergo considerable changes: we can observe some O—O pairs with very small interatomic distances, which are taken into account in the first maximum at the $D(r)$ curve. The consequence of that is the tendency to larger W—O distances and to greater dispersion of the values of the distances in the melted relaxed atomic configuration. The W—O distances for the crystal and for the initial cluster are about 1.9 Å.

The change in the values of effective charges during the calculation of the W—O interaction potential results in the displacement of the potential well bottom from 1.94 Å to 1.8 Å at $z_W = 4.2$ and $z_O = -1.25$, and to 1.7 Å at $z_W = 4.73$ and $z_O = -1.42$. The ionization degree of the bonds with these charge values is 0.7 and 0.79, respectively. The values of the charges used to calculate the Coulomb repulsion part of the W—W and O—O potentials were taken as 3.36 and −1.12, respectively. There are always O atoms placed between the W—W pairs, which reduces the Coulomb repulsion between the W atoms. It was also established that, with these changes in the effective charges of the W—O interaction, the first maximum of the $D(r)$ curve calculated for the melted not-relaxed cluster moves towards lower $r$ at $\Delta r_{W-O} = 0.1$ Å each time. Nevertheless, it does not achieve the position corresponding to the experimental one. This happens because the interatomic distances for all pairs of atoms decrease, but as a whole the distribution of the distances does not change: we still have distances with values not corresponding to the crystallochemical conditions and, moreover, W—W pairs with small (3.22 Å and 3.37 Å) distances appear.

At the next stage the melting of the cluster was carried out using the next interaction potentials: W—O, calculated at $z_W = 4.73$, $z_O = -1.42$ (potential well bottom at 1.7 Å), and W—W, calculated at $z_W = 4.3$. After that, the W—W distance increased from 3.22 Å to 3.64 Å, which is close to the experimental values for the respective distances in the amorphous and crystalline $WO_3(1/3)H_2O$ phase.

Since the O—O distances in the atomic configuration are small using these interaction potentials, at the next stage of the model construction the charge $z_O$ in the Coulomb part of the O—O interaction potential was increased to −1.3. This did not cause considerable changes in the maximums of the $D(r)$ curve. The distances between the oxygen pairs changed: on the one hand, the average radius of the first coordination O—O sphere increased, but, on the other, a very small quantity of pairs with ever decreasing distances appeared. This had the same effect on the W—O distances. The radius distribution of the W—W coordination spheres stayed almost the same. During the relaxation of such a melted atomic configuration, O—O and W—W pairs with very small distances disappear. At the same time, the W—W distances in the relaxed melted cluster spread more than in the not-relaxed one.

Since the increment in the oxygen charge in the O—O interaction potential does not improve the distribution of the distances, $z_O$ for the Coulomb interaction of oxygen was taken as −1.12 for the next simulations.

For the W—W interaction potential, the charge $z_W$ was taken as 4.3 and the position of the bottom of the potential well for the W—O interaction was fixed at 1.8 Å. With these potential values, the influence of the cutoff on the final atomic configuration was investigated. It is known that a good accordance between experiments and the simulation of amorphous metals and alloys can be achieved using a short cutoff (Polukhin & Vatolin, 1985).

A cutoff for the O—O interaction potential equal to $r_c = 2.8$ Å results in a small increment in the dispersion of W—O and O—O distances and the spreading of the W—W system between 3.4 Å and 4.1 Å; the average W—W distance remains 3.64 Å. Cutting only the W—W potential leads to the spread of all the spheres and a decrement in the average distances, especially for the W—W pairs, where the average

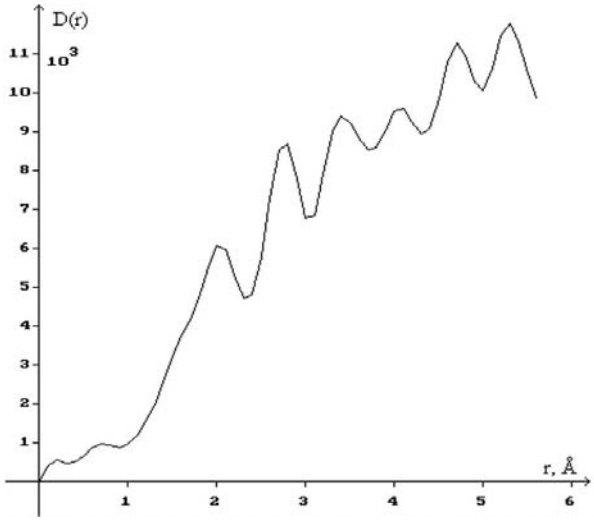


**Figure 6**
The distribution curve of pair functions $D(r)$ calculated for the melted not-relaxed initial configuration simulated for $WO_3$ (256 atoms).

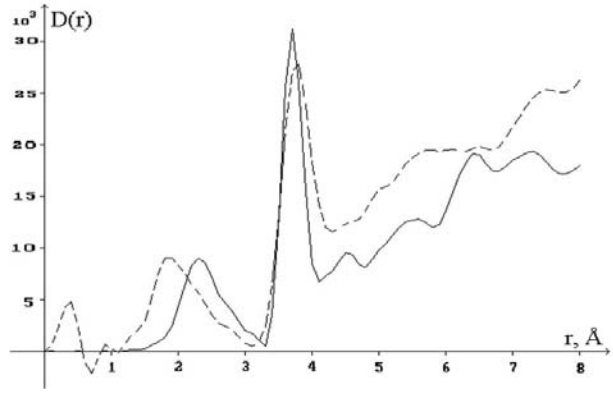


**Figure 7**
The distribution curves of pair functions $D(r)$: the dashed line corresponds to the experimental curve for the $WO_3$ oxide films; the solid line corresponds to the curve calculated for the melted relaxed configuration simulated for $WO_3$ (256 atoms). The Coulomb part of the potential is calculated using the effective charge values $z_W = 3.36$, $z_O = -1.12$; the cutoff is equal to one-quarter of the linear size of the model.

distance becomes 2.81 Å instead of 3.65 Å. The maxima of the $D(r)$ curve are displaced towards smaller $r$.

The cooling of the melted relaxed model and the relaxation of the cooled model did not change the distribution of the $D(r)$ curves of pair functions calculated in these cases. Previously, similar results were obtained for molecular dynamics simulations of amorphous $Al_2O_3$ and $Na_2O-WO_3$ structures (Buhtoiarov & Voronova, 1989; Belaschenko, 1994).

The first maximum of the $D(r)$ curve that corresponds to W—O pairs coincides with the experimental one if we decrease the cutoff of the W—O potential to 2.8 Å (Fig. 8). For this case, the maximum that corresponds to the W—W pairs also coincides with the experimental one. Using this cutoff for the W—O potential, the nearest distance for the O—O atoms increases to 2.26 Å.

The first maximum of the $D(r)$ curve calculated for the model configuration closely resembles the first maximum of the experimental $D(r)$ curve for the $WO_3$ oxide films obtained by thermal evaporation of $WO_3$ powder in a vacuum (Fig. 8*a*). However, the behaviour of $D(r)$ calculated for the model configuration at the range beyond the first maximum is in poor agreement with the experimental $D(r)$ curve for this oxide. The discrepancy between both of the experimental distribution curves $D(r)$ for the anodic amorphous oxide and the similar distribution curves calculated for the model configuration $WO_3$ is pronounced (Fig. 8*b*). The intensity $I(s)$ curves are illustrated in Fig. 9.

Fig. 10 shows part of the atomic configuration (projected onto the *ab* plane) constructed during the molecular dynamics experiment for $WO_3$ oxide. We can see a chain of distorted octahedra similar to those existing for the crystal $ReO_3$-type phase.

Thus, the best-fitting distribution curves [$D(r)$ and $I(s)$] calculated for the model configuration $WO_3$ are obtained with the following molecular dynamic simulation conditions: effective charge values $z_W = 4.3$, $z_O = -1.12$; W—W and O—O cutoff ($r_{c\,W-W}$ and $r_{c\,O-O}$) at one-quarter of the box lengths; W—O cutoff potential $r_{c\,W-O} = 2.8$ Å. The medium

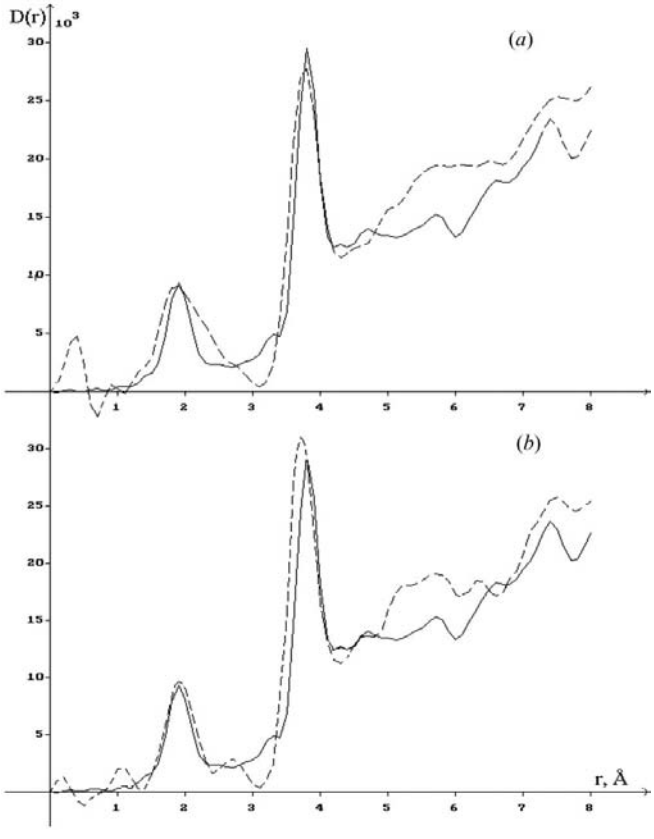


**Figure 8**
The distribution curves of pair functions $D(r)$: the dashed line corresponds to the experimental curve (*a*) for the $WO_3$ oxide films obtained by thermal evaporation of $WO_3$ powder in a vacuum and (*b*) for the anodic $WO_3$ oxide films; the solid line corresponds to the curve calculated for the relaxed melted configuration simulated for $WO_3$ (256 atoms). The Coulomb part of the potential had the effective charge values $z_W = 4.3$, $z_O = -1.12$; the W—W and O—O cutoff of the potentials is equal to one-quarter of the linear size of the model; the W—O cutoff $r_{c\,W-O} = 2.8$ Å.

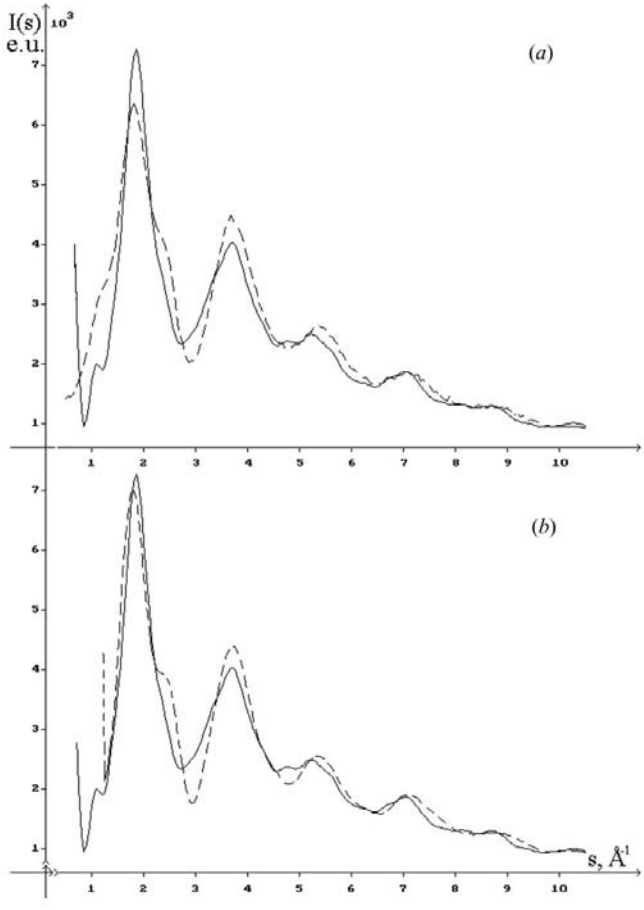


**Figure 9**
The distribution curves of scattering intensity $I(s)$: the dashed line corresponds to the experimental curve (*a*) for the $WO_3$ oxide films obtained by thermal evaporation of $WO_3$ powder in a vacuum and (*b*) for the anodic $WO_3$ oxide films; the solid line corresponds to the curve calculated for the relaxed melted configuration simulated for $WO_3$ (256 atoms, $z_W = 4.3$, $z_O = 1.12$; the W—W and O—O cutoff of the potential is equal to one-quarter of the linear size of the model; the W—O cutoff $r_{c\,W-O} = 2.8$ Å).

pressure of the system during the relaxation at room temperature was 0.15 GPa.

### 5.2. $WO_{3+1/3}$ configuration

The short-range-order characteristics presented in Table 2 show that the atomic arrangement of the anodic amorphous oxide $WO_3$ corresponds to that of the $WO_3(1/3)H_2O$ phase. Consequently, we had to increase the number of O atoms in the model configuration in order to simulate the $WO_{3+1/3}$ configuration.

The $WO_{3+1/3}$ configurations consisted of 208 atoms (160 O atoms and 48 W atoms, 48 formula units of $WO_3$) and 624 atoms (480 O atoms and 144 W atoms, 144 formula units of $WO_3$) of W and O placed inside a cube with linear dimensions dependent on the model density.

Initially, the molecular dynamics simulation conditions for which we obtained the best agreement for the distribution curves [$D(r)$ and $I(s)$] calculated for the model configuration $WO_3$ were used: effective charge values $z_W = 4.3$, $z_O = -1.12$; W—W and O—O cutoff potentials at one-quarter of the box lengths; $r_{c\,W-O} = 2.8$ Å.

The agreement between the experimental distribution pair functions $D(r)$ and scattering intensity $I(s)$ for the anodic amorphous oxide $WO_3$ and the model $D(r)$ and $I(s)$ curves calculated for the last configuration is much better than in all the previous cases. However, the maxima of the model curves are narrower than the experimental curves (Figs. 11 and 12).

Therefore, the atomic configuration size was increased and the changes in the $D(r)$ and $I(s)$ curves were analyzed. It was established that the $D(r)$ and $I(s)$ curves (Figs. 13 and 14) practically coincide with the experimental ones for the 624-atom cluster with $WO_{3+1/3}$ composition under the following conditions: $z_W = 4.3$, $z_O = -1.12$, $r_{c\,W-O} = 2.8$ Å, $r_{c\,O-O} = 5$ Å, $r_{c\,W-W} = 3.7$ Å, density 6.5 g cm$^{-3}$. The medium pressure of the system during the relaxation at room temperature was 0.15 GPa.

Figs. 15(*a*) and 15(*b*) show the fragments of the 208-atom and 624-atom configurations constructed during the molecular dynamics experiment. The scattering intensity distribution curves are practically the same as the experimental ones (Figs. 13 and 14).

We can see that the configuration consists of octahedra, forming hexagonal rings similar to those in crystalline $WO_3(1/3)H_2O$ but more distorted. In the dashed octahedra in some of the rings, the O atom, which must be located on the octahedron axis, is missing.

In Table 4, the average interatomic distances and the total coordination numbers calculated using the periodical boundary conditions for the cooled relaxed model clusters with $WO_{3+1/3}$ composition for 208 atoms and 624 atoms are compared with the experimental data for the amorphous anodic tungsten oxide powder.

The Table 4 analysis and Fig. 15 show that some of the W and O atoms in the models form $WO_5$ polyhedra, and the first

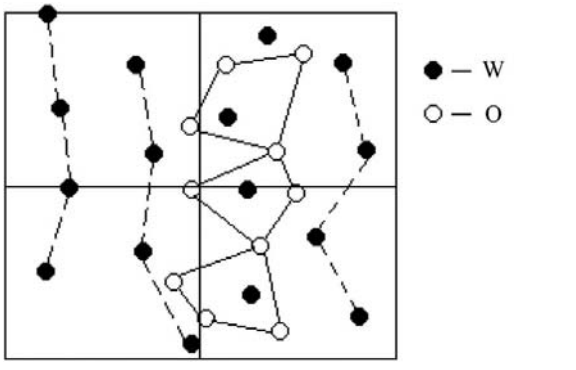


**Figure 10**
The chains formed by the oxygen octahedra in the cooled relaxed cluster with $WO_3$ composition (256 atoms), *xy* plane.

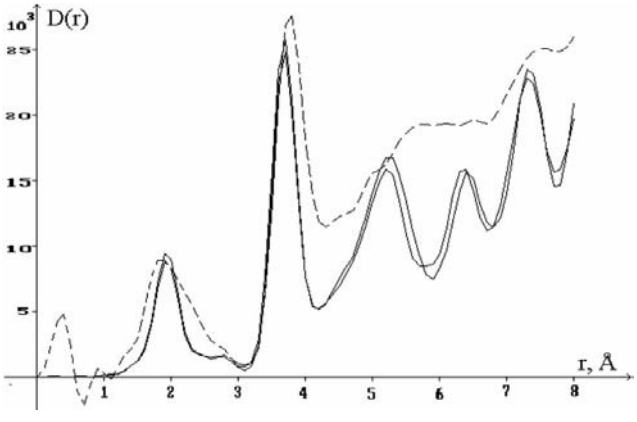


**Figure 11**
The distribution curves of pair functions $D(r)$: the dashed line corresponds to the anodic oxide, the solid lines correspond to the melted not-relaxed and relaxed cooled configurations $WO_{3+1/3}$ (208 atoms) simulated by the molecular dynamics method ($z_W = 4.3$, $z_O = -1.12$; the W—W and O—O cutoff was taken to be one-quarter of the linear size of the model; the W—O cutoff $r_{c\,W-O} = 2.8$ Å).

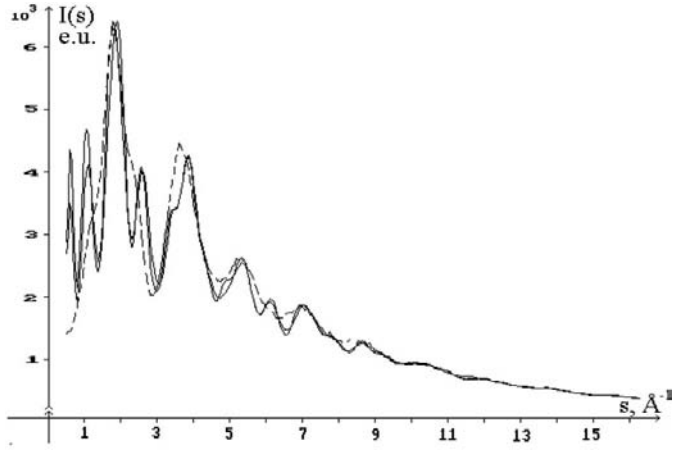


**Figure 12**
The distribution curves of scattering intensity $I(r)$: the dashed line corresponds to the anodic oxide, the solid lines correspond to the melted not-relaxed and relaxed cooled configurations $WO_{3+1/3}$ (208 atoms) ($z_W = 4.3$, $z_O = -1.12$; the W—W and O—O cutoff was taken to be equal to one-quarter of the linear size of the model; the W—O cutoff $r_{c\ W-O} = 2.8$ Å).

**Table 4**
Results of the average interatomic distances and the total coordination numbers calculated for the model configuration $WO_{3+1/3}$.

| | Amorphous powder sample experimental data† $r_{ij}$ (Å) ($\Delta r$ = 0.01 Å) | $N_{ij}$ (atoms) | Relaxed cooled cluster $WO_{3+1/3}$, 208 atoms $r_{ij} \pm \Delta r$ (Å) | $N_{ij}$ (atoms) | Relaxed cooled cluster $WO_{3+1/3}$, 624 atoms $r_{ij} \pm \Delta r$ (Å) | $N_{ij}$ (atoms) |
|---|---|---|---|---|---|---|
| W—O | 1.85 | 5.4 ± 0.01 | 1.89 ± 0.1 | 4.4 | 1.922 ± 0.1 | 4.2 |
| W—O | 2.22 | 1.6 ± 0.05 | 2.03 ± 0.03 | 1.4 | 2.089 ± 0.1 | 1.7 |
| O—O | 2.65 | 17.0 ± 0.6 | 2.80 ± 0.4 | 7.7 | 2.798 ± 0.45 | 7.7 |
| W—W | 3.72 | 4.0 ± 0.3 | 3.70 ± 0.15 | 3.8 | 3.73 ± 0.2 | 4.9 |
| W—W | 3.81 | 1.4 ± 0.3 | 3.98 ± 0.1 | 1.7 | 4.01 ± 0.2 | 0.9 |

† Aleshina & Lugovskaya (1997).

total coordination number has a more understanding value in comparison with the experimental one. It must be mentioned that the more lower value of the first W—O and the O—O coordination numbers in comparison with the experimental one for the anodic amorphous powder is the result of the absence of hydrogen in the model configurations. The long W—O distances (2.03 Å and 2.089 Å) correspond to the bond between the W atoms and O atoms that belong to water molecules.

As a consequence of the absence of O atoms in some octahedra, the average O—O distance (equal to 2.80 Å) is high compared with the experimental one, $r_{O-O}$ = 2.65 Å. The average distance and the coordination number for the first W—W sphere of the 208-atom cluster corresponds to the value obtained from the experimental $D(r)$ curve for the anodic oxide powder. The second W—W distance in both models is larger than that calculated from the experimental $D(r)$ curve. In the 624-atom model, we can observe more W—W pairs with a distance of 3.73 Å (which coincides with the experimental results) and fewer pairs with distances of about 4 Å than in the 208-atom cluster. The dispersion of the distances is about the average experimental spread.

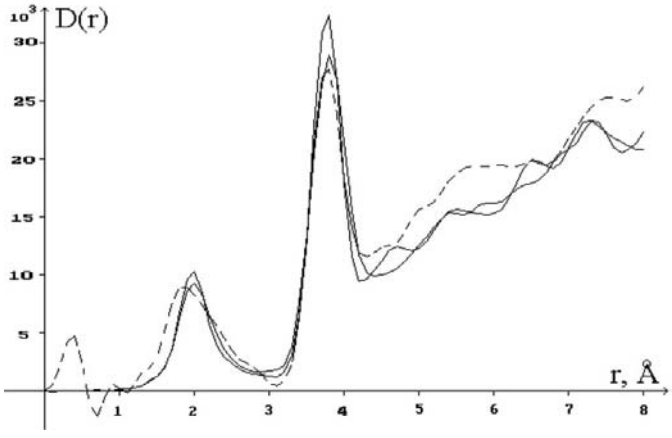


**Figure 13**
The pair function curves $D(r)$ for the anodic oxide powder (dashed line), not-relaxed melted cluster and relaxed cooled cluster (solid lines) consisting of 624 atoms ($z_W$ = 4.3, $z_O$ = −1.12; the W—O cutoff $r_{c\,W-O}$ = 2.8 Å; the O—O cutoff $r_{c\,O-O}$ = 5 Å; the W—W cutoff $r_{c\,W-W}$ = 3.7 Å).

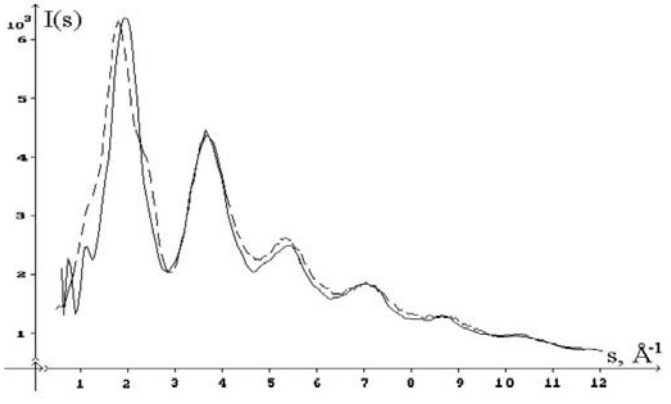


**Figure 14**
The scattering intensity distribution curves $I(r)$ for anodic oxide powder (dashed lines) and the relaxed cooled 624-atom cluster $WO_{3+1/3}$ (solid line) ($z_W$ 4.3, $z_O$ = −1.12; the W—O cutoff $r_{c\,W-O}$ = 2.8 Å; O—O cutoff $r_{c\,O-O}$ = 5 Å, W—W cutoff $r_{c\,W-W}$ = 3.7 Å).

## 6. Conclusions

The X-ray study of amorphous anodic tungsten oxide showed that the arrangement of W and O atoms at the coordination spheres corresponds to that characteristic for the crystalline $WO_3(1/3)H_2O$ modification. $WO_3$ films, obtained by thermal evaporation in a vacuum, have a quasi-amorphous structure. The structure is characterized by the presence of crystallites shaped mainly as orthorhombic-phase parallelepipeds with dimensions 15 × 8 × 20 Å.

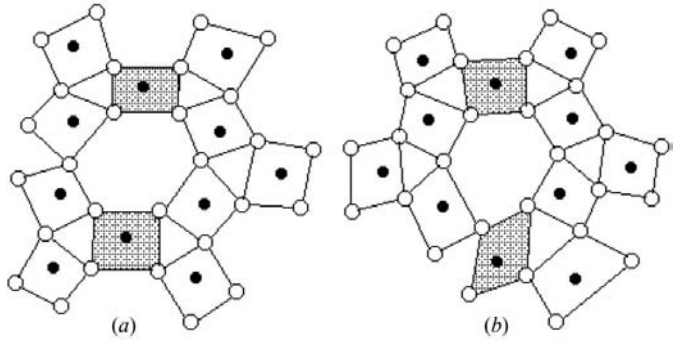


**Figure 15**
Hexagonal ring formed by the oxygen octahedra in the cooled relaxed cluster with $WO_{3+1/3}$ composition for 208 (*a*) and 624 (*b*) atoms, *xy* plane.

The computer simulation of the structure of tungsten oxide carried out by the molecular dynamics method showed that the tungsten subsystem can be well reproduced using a cutoff potential of about 4 Å, but, in the oxygen subsystem with this cutoff, interatomic distances for W—W, W—O and O—O pairs appear to be lower than the O-atom diameter. The nearest O—O distance becomes equal to the sum of the O atoms' radii only when we decrease the cutoff of the potential for the W—O pairs to 2.8 Å.

Chains of distorted octahedra can be observed in the molecular dynamics experiment for the $WO_3$ models. The arrangement of these chains is similar to that of the crystalline $ReO_3$-type phase. The calculated scattering intensity distribution for the 256-atom configuration shows a satisfactory agreement with the experimental one for the oxide obtained by thermal evaporation of $WO_3$ powder in a vacuum.

Addition of (1/3)O for each unit of composition results in the octahedra forming hexagonal rings of the same type as in the $WO_3(1/3)H_2O$ phase but more distorted. The calculated scattering intensity distribution for the configuration from 624 atoms has a satisfactory agreement with the experimental one for the anodic tungsten oxide powder.

This work was support by fundamental fund 'Russian University'.

## References


Aleshina, L. A. & Fofanov, A. D. (1987). *Rentgenostruktumyi Analiz Amorfnykh Materialov* (*X-ray Analysis of Amorphous Materials)*, p. 84. Petrozavodsk: Petrozavodsk University.

Aleshina, L. A., Fofanov, A. D. & Shivrin, O. N. (1982). *Dokl. Akad. Nauk SSSR*, **267**, 596–598.

Aleshina, L. A., Glazkova, S. V., Lugovskaya, L. A., Malinenko, V. P. & Fofanov, A. D. (1998). *Russ. J. Electrochem.* **34**, 988–994.

Aleshina, L. A. & Lugovskaya, L. A. (1997). *Cryst. Rep.* **42**, 303–309.

Aleshina, L. A., Malinenko, V. P., Phouphanov, A. D. & Yakovleva, N. M. (1986). *J. Non-Cryst. Solids*, **87**, 350–360.

Aleshina, L. A. & Nikitina, E. A. (1992). *Modelirovanie Struktury Amorfnykh Okislov Alyuminiya Metodom Razmyvaniya Kristallicheskoi Reshetki* (*Modeling of the Structure of Amorphous Aluminium Oxides by the Method of the Crystal-Lattice Blurring*). VINITI, Moskva, N 2524-B92.

Aleshina, L. A., Vakulin, D. V. & Nikitina, E. A. (1995). *Zavod. Lab.* **6**, 31–33.

Andersen, H. C. (1980). *J. Chem. Phys.* **72**, 2384–2393.

Belaschenko, D. K. (1994). *Neorg. Mater.* **30**, 948–954.

Bokii, G. B. (1971). *Kristallohimia* (*Crystal Chemistry*), p. 400. Moskva: Nauka.

Buhtoiarov, O. I. & Voronova, L. I. (1989). *Rasplavi*, N**4**, 60–64.

Deb, S. K. (1969). *Appl. Optics Suppl. Electrophotogr.* **7**, 192–195.

De Wijs, G. A. & De Groot, R. A. (1999). *Phys. Rev. B*, **60**, 16463–16473.

Falaras, P., Froelicher, M., Froment, M., Hugot, U. & Goff, A. (1984). *J. Microsc. Spectrosc. Electr.* **9**, 39–45.

Fillipchenko, V. Ya., Finkel'shtein, S. Kh. & Surov, Yu. I. (1980). *Izv. Akad. Nauk SSSR Neorg. Mater.* **16**, 1687–1693.

Finbak, C. & Borgen, O. (1954). *Acta Chem. Scand.* **8**, 829–834.

Fofanov, A. D. (1998). DSc thesis, Moscow State University, Russia.

Forsythe, G. E., Malcolm, M. A. & Moler, C. B. (1977). *Computer Methods for Mathematical Computations*. Englewood Cliffs, NJ: Prentice-Hall.

Gerand, B., Nowogrocki, G. & Figlarz, M. A. (1981). *J. Solid State Chem.* **38**, 312–320.

Gerand, B., Nowogrocki, G., Guenot, J. & Figlarz, M. A. (1979). *J. Solid State Chem.* **29**, 429–434.

Gorbunov, O. B., Surov, Yu. I., Totokin, V. R., Fillipchenko, V. Ya. & Finkel'shtein, S. Kh. (1981). *Poluchenie i Svoistva Tonkikh Plenok* (*Synthesis and Properties of Thin Films*), p. 52. Kiev: Naukova Dumka.

Gutierrez, G., Belonoshko, A. B., Ahuja, R. & Johansson, B. (2000). *Phys. Rev. E*, **61**, 2723–2729.

Gutierrez, G. & Johansson, B. (2002). *Phys. Rev. B*, **65**, 12101–12104.

Hockney, R. W. & Eastwood, J. W. (1981). *Computer Simulation Using Particles*, p. 640. New York: McGraw-Hill.

Kalibaeva, G. M. (1992). PhD thesis, Moscow State University, Russia.

Lawson, C. L. & Hanson, R. J. (1974). *Solving Least Squares Problems*. Englewood Cliffs, NJ: Prentice-Hall.

Lugovskaya, L. A. (2000). PhD thesis, Moscow State University, Russia.

Olevskii, S. S., Sergeev, M. S., Tolstikhina, A. L., Avilov, A. S., Shkornyakov, S. M. & Semiletov, S. A. (1984). *Dokl. Akad. Nauk SSSR*, **275**, 1415–1419.

Palatnic, L. S., Obolianinova, O. A. & Naboka, M. N. (1973). *Izv. Akad. Nauk SSSR Neorg. Mater.* **9**, 801–804.

Paola, A., Quarto, F. & Sunsert, G. (1978). *J. Electrochem. Soc.* **125**, 1344–1347.

Parinello, M. & Rahman, A. (1981). *J. Appl. Phys.* **52**, 7182–7190.

Polukhin, V. A. & Vatolin, N. A. (1985). *Modelirovanie Amorfnikh Metallov* (*Modeling of Amorphous Metals*), p. 288. Moskva: Nauka.

Rappe, A. K., Casewit, C. J., Colwell, K. S., Goddard, W. A. III & Skiff, W. M. (1992). *J. Am. Chem. Soc.* **114**, 10024–10035.

Shiojri, M. & Migano, T. (1980). *Tech. Appl. Cannes.* **1**, 413–417.

Skrishevskii, A. F. (1980). *Structurnii Analiz Zhidkostei i Amorfnih Tel*, p. 328. Moskva: Visshaia shkola.

Stepanyuk, V. S., Katsnelson, A. A., Kalibaeva, G. M. & Szasz, A. (1991). *Fizica Tverdogo Tela* (*Sov. Phys. Solid State*), **10**, 3095–3097.

Stepanyuk, V. S., Szasz, A., Katsnelson, A. A. & Trushin, O. S. (1991). *J. Non-Cryst. Solids*, **130**, 311–318.

Udalova, V. V. & Klechkovskaya, V. V. (1986). *Kristallograftya i Kristallokhimiya* (*Crystallography and Crystal Chemistry*), p. 224. Moskva: Nauka.

Urusov, V. S. (1975). *Energeticheskaya Kristallohimia*, p. 335. Moskva: Nauka.

Warren, B. E. (1969). *X-ray Diffraction*, p. 630. Reading, MA: Addison-Wesley.